AIAA JOURNAL
Vol. 48, No. 11, November 2010

Technical Notes

How Does a Gurney Flap Enhance the Aerodynamics Forces?

Yang-Yao Niu* and Ting-Shiu Hsu
Chung-Hua University,
Hsin-Chu 30067, Taiwan, Republic of China
and
C. T. Hsieh, C. C. Chang, and C. C. Chu
National Taiwan University,
Taipei 106, Taiwan, Republic of China

DOI: 10.2514/1.J050437

Nomenclature

C_D	=	total drag coefficient
C_{Da}	=	drag coefficient associated with the acceleration of the wing
C_{Dm}	=	drag coefficient associated with the motion of the wing
C_{Ds}	=	drag coefficient associated with the surface vorticity and friction on the wing surface
C_{Dv}	=	drag coefficient associated with to vorticity within the flowfield
C_L	=	total lift coefficient
C_{La}	=	lift coefficient associated with the acceleration of the wing
C_{Lm}	=	lift coefficient associated with the motion of the wing
C_{Ls}	=	lift coefficient associated with the surface vorticity and friction on the wing surface
C_{Lv}	=	lift coefficient associated with to vorticity within the flowfield
c^*	=	chord length
P^*	=	static fluid pressure
Re	=	Reynolds number
$U^*_{\max}$	=	maximum velocity
$\mathbf{u}$	=	velocity vector
μ^*	=	air viscosity
ρ^*	=	air density
ϕ	=	auxiliary potential function
$\boldsymbol{\omega}$	=	vorticity

Introduction

STUDY of low-speed aerodynamics, especially high-lift system performance, has a major influence on the design and safety of any airplane configuration. As noted in [1], the Stratford criterion [2] was applied by Smith [3] and Leibeck [4] to design multi-element airfoils for achieving maximum lift. The shape design of each element in high-lift airfoils requires maximum pressure difference between the upper and lower surfaces of each element in order to increase the upper surface suction and lower pressure. One common passive method for lift enhancement is to add a short 90 deg inverted flat plate at the trailing edge of the airfoils. This is called a Gurney flap; it was originally used on a racing car by Daniel Gurney in the 1970s. As Leibeck first hypothesized, a Gurney flap can increase the lift by deflecting the flow at the trailing edge. In fact, a tab like the Gurney flap can be mounted on any element in multi-element high-lift systems to increase the load of the main element and delay flow separation on the flap. With a Gurney flap, the aerodynamic force alteration is associated with a small region of separated airflow upstream of the flap, with two counter-rotating vortices downstream of the flap effectively modifying the trailing-edge Kutta condition, resulting in a finite pressure difference between the upper and lower surfaces at the trailing edge. To understand the enhanced aerodynamics produced by the Gurney flap, Wadcock [5] performed two-dimensional wind-tunnel tests at a Reynolds number of 1.64×10^6 on a baseline NACA 4412 airfoil at the NASA Ames 7 by 10 Foot Wind Tunnel. These tests showed that a Gurney flap with a 1.25% chord length significantly increased the lift coefficient, shifting the lift curve up by 0.3, thus providing a higher maximum lift. There was no appreciable increase in drag until the Gurney flap height was increased beyond about 2% of the airfoil chord length. Storms and Jang [6], who conducted an experimental study on the same airfoil with Gurney flap, reported similar trends. However, they observed that though there is good correlation between experimental and computational lift coefficients obtained by Jang et al. [7] for a clean airfoil, computations seem to underpredict the lift increment caused by the Gurney flap. Jang et al. [7] used an incompressible Navier–Stokes code to compute the flowfield of the NACA 4412 airfoil with Gurney flap heights ranging from 0.5 to 3% of the chord. These computations predicted an increase in the lift coefficient and nose-down pitching moment. They also show that at moderate angles of attack, the Gurney flap causes separation points on the suction surface to shift aft, compared to the clean airfoil. They noticed an increase in load increments along the entire length of the airfoil when the Gurney flap is used. Laser Doppler anemometry measurements by Jeffrey et al. [8] and time-averaged particle image velocimetry analysis by Solovitz and Eaton [9,10] gave additional information on the flow pattern around Gurney flaps. Flap application to unmanned air vehicles was particularly studied. The purpose of the present study is work is to solve the unsteady two-dimensional Navier–Stokes equations [11,12] coupled with a force-element theory [13] to distinguish the contributions of individual fluid elements to the aerodynamic enhancements produced by a Gurney flap on a NACA 4412 airfoil. The force-element theory proposed by Chang [13] is briefly described in the next section.

Numerical Models and Discussions

To analyze the various contributions to the force on a finite body in a flow, we need to introduce auxiliary potential solutions [13,14]. Let us first describe the nature of these potential solutions. A potential solution φ satisfies $\nabla^2\phi = 0$ and is required to vanish at infinity, which the fluid is assumed to be at rest. In two dimensions, at great distance r from the body, a potential solution is given by

$$\phi = -(\mathbf{B}\cdot\nabla)\log\mathbf{r} + \cdots = -\frac{\mathbf{B}\cdot\mathbf{r}}{\mathbf{r}} + \cdots \tag{1}$$

where r is the unit vector in the direction of the position vector. The constant vector $\mathbf{B}$ depends on the shape and direction of motion of the wing assumed for a specific solution φ. To find $\mathbf{B}$, it requires a complete solution of the equation $\nabla^2\phi = 0$ [15] and appropriate boundary conditions. It should be kept in mind that the corresponding velocity $\nabla\varphi$ decays like $1/r^2$ in two dimensions. The assumed direction of motion and corresponding boundary conditions

Received 9 March 2010; revision received 23 July 2010; accepted for publication 25 July 2010.

*Professor, Department of Mechanical Engineering; yniu@chu.edu.tw (Corresponding Author).

depend on which force direction is considered. If S is the unit vector along the force direction of interest, then we require $n \cdot \nabla\varphi = -n \cdot S$ on the body surface. The potential solution that satisfies this boundary condition is used to decompose the force in the S direction for motion through the real viscous fluid into an added-mass force, a surface vorticity force, and a volume vorticity force, as well as other possible contributions.

Consider a single airfoil moving through air. Let ρ^* be the air density; μ^* is the air viscosity, c^* is the chord length of the airfoil, and $U^*_{\max}$ is the maximum velocity. Take $c^*/2$ to be the reference length, $c^*/2U^*_{\max}$ to be the reference time and p^* to be the static pressure related to $p^* = \rho^* U^{*2}_{\max} P$. The flowfield is assumed to be governed by the Navier–Stokes equations and incompressibility condition, which are given in dimensionless form by

$$\frac{\partial \mathbf{u}}{\partial t} + (\mathbf{u} \cdot \nabla)\mathbf{u} = -\nabla p + \frac{2}{Re}\nabla^2 \mathbf{u} \tag{2}$$

$$\nabla \cdot \mathbf{u} = 0 \tag{3}$$

where u is the velocity vector and $Re = \rho^* c^* U_{\max}/\mu^*$ is the Reynolds number. A well-known formula for calculating the lift is

$$C_L = \int_S p\mathbf{n} \cdot \mathbf{j}\, \mathrm{d}A + \frac{2}{Re}\int_S \mathbf{n} \times \boldsymbol{\omega} \cdot \mathbf{j}\, \mathrm{d}A \tag{4}$$

where j is the unit vector in the lift direction, n is the inward vector normal to the airfoil surface, and ω denotes the vorticity vector. Now we show how to obtain the formulas for the force on the airfoil according to the force-element method. Lift will be done first. Equation (2) can be written as

$$-\nabla p = \frac{\partial \mathbf{u}}{\partial t} + \frac{1}{2}\nabla|\mathbf{u}|^2 - \mathbf{u} \times \boldsymbol{\omega} + \frac{2}{Re}\nabla \times \boldsymbol{\omega} \tag{5}$$

The procedure is to take a dot product of this equation with the gradient of a potential flow solution φ as described above, in which the airfoil motion is in the direction of the lift. This dot product is then integrated over a volume V_R outside the wing surface S, but within a cylindrical surface S_R of a large radius R. Here, we use the two identities as $\mathbf{u} \cdot \nabla\phi = \nabla \cdot (\mathbf{u}\phi)$ and $(\nabla \times \boldsymbol{\omega}) \cdot \nabla\phi = \nabla(\boldsymbol{\omega} \times \nabla\phi)$ and apply the divergence theorem. This yields

$$-\int_{\mathrm{SUS}_R} p\mathbf{n} \cdot \nabla\phi\, \mathrm{d}A = \int_{\mathrm{SUS}_R} \phi\frac{\partial \mathbf{u}}{\partial t} \cdot \mathbf{n}\, \mathrm{d}A + \frac{1}{2}\int_{\mathrm{SUS}_R} |\mathbf{u}|^2 \nabla\phi \cdot \mathbf{n}\, \mathrm{d}A$$
$$-\int_{V_R} \mathbf{u} \times \boldsymbol{\omega} \cdot \nabla\phi\, \mathrm{d}V + \frac{2}{Re}\int_{\mathrm{SUS}_R} \mathbf{n} \times \boldsymbol{\omega} \cdot \nabla\phi\, \mathrm{d}A \tag{6}$$

The force-element method uses a coordinate system in which the fluid is at rest far from the body. Applying this boundary condition and noting that $\nabla\phi$ decays like $1/r^2$, we can carry out the integral on the left-hand side and the first, second, and fourth ones on the right-hand side with $R \to \infty$ and $V_R \to V$ (entire fluid region) to obtain

$$-\int_S p\mathbf{n} \cdot \nabla\phi\, \mathrm{d}A = \int_S \phi\frac{\partial \mathbf{u}}{\partial t} \cdot \mathbf{n}\, \mathrm{d}A + \frac{1}{2}\int_S |\mathbf{u}|^2 \nabla\phi \cdot \mathbf{n}\, \mathrm{d}A$$
$$-\int_V \mathbf{u} \times \boldsymbol{\omega} \cdot \nabla\phi\, \mathrm{d}V + \frac{2}{Re}\int_S \mathbf{n} \times \boldsymbol{\omega} \cdot \nabla\phi\, \mathrm{d}A \tag{7}$$

The boundary condition for ϕ on the body surface is the left side; using this boundary condition in the left-hand side above gives

$$-\int_S p\mathbf{n} \cdot \nabla\phi\, \mathrm{d}A = \int_S p\mathbf{n} \cdot \mathbf{j}\, \mathrm{d}A$$

Finally, if the frictional force

$$\frac{2}{Re}\int_S \mathbf{n} \times \boldsymbol{\omega}\, \mathbf{j}\, \mathrm{d}A$$

[i.e., the second term on the right-hand side of Eq. (4)] is included, the complete decomposition for the lift force can be obtained:

$$C_L = C_{La} + C_{Lm} + C_{L\upsilon} + C_{Ls} \tag{8}$$

where

$$C_{La} = \int_S \phi\frac{\partial \mathbf{u}}{\partial t} \cdot \mathbf{n}\, \mathrm{d}A; \qquad C_{Lm} = \frac{1}{2}\int_S |\mathbf{u}|^2 \nabla\phi \cdot \mathbf{n}\, \mathrm{d}A$$
$$C_{L\upsilon} = -\int_V \mathbf{u} \times \boldsymbol{\omega} \cdot \nabla\phi\, \mathrm{d}V; \qquad C_{Ls} = \frac{2}{Re}\int_S \mathbf{n} \times \boldsymbol{\omega} \cdot (\nabla\phi + \mathbf{j})\, \mathrm{d}A \tag{9}$$

In Eq. (9), C_{La} is the contribution by the acceleration of the wing; C_{Lm} corresponds to the contribution by the velocity of the wing; C_{Ls} denotes the contribution by the surface vorticity and friction on the wing surface; and $C_{L\upsilon}$ represents the contribution of pressure force due to vorticity within the flowfield. In $C_{L\upsilon}$, the integrand $-\mathbf{u} = \boldsymbol{\omega} \cdot \nabla\phi$ is called the volume lift-element density, and

$$(2/Re)\int_S \mathbf{n} \times \boldsymbol{\omega} \cdot (\nabla\phi + \mathbf{j})\, \mathrm{d}A$$

is called the surface lift-element density, where the part with $\nabla\phi$ is called the frictionlike force. Either of them may be termed the vortex force-element density. A salient feature is that only the volume lift elements near the body contribute significantly to the lift force, because $\nabla\phi$ decays fairly rapidly away from the body. The potential function ϕ can be considered as a geometric factor, because each flow condition can be associated with a unique ϕ. Note that among the force components, C_{La} and C_{Lm} are determined by the boundary conditions and the geometric profile, while the determination of $C_{L\upsilon}$ and C_{Ls} requires solution of the fluid flow. Note that if we consider the force in drag direction (say, $S = i$), then ϕ has to satisfy $n \cdot \nabla\phi = -n \cdot i$ on the wing surface. Following the same procedure as in Eqs. (5–7), we can derive that the force along the i direction is decomposed by

$$C_D = C_{Da} + C_{Dm} + C_{D\upsilon} + C_{Ds} \tag{10}$$

In the present work, the test flow is taken following [6] to be a two-dimensional stationary NACA 4412 airfoil at a zero angle of attack, with a 0.085 Mach number, and a Reynolds number of 1.64×10^6, corresponding to different Gurney flap sizes of 0.5 to 7% airfoil chord length. To validate our computation, a satisfactory comparison with the experimental surface pressure data from [6] on the clean NACA 4412 airfoil is shown in Fig. 1.

Figure 1 also includes a grid independence study. One of the used structured grids shown in the figure as 250×80 is considered to be fine enough for the further simulation. A 0.9 of Courant–Friedrichs–Lewy number was chosen to give enough numerical stability to achieve steady-state solutions. In the study of the Gurney flap effects, the lift and drag (C_{Da}, C_{Dm}, C_{La}, and C_{Lm}) induced by body motion and acceleration are zero, because the airfoil has constant velocity. In our simulations, as shown in Fig. 2 and Tables 1–3, the lift and the lift-to-drag ratio are obviously enhanced by the Gurney flap. As is

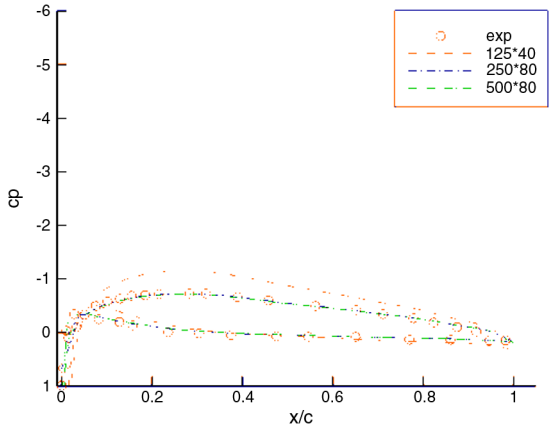

Fig. 1 Numerical validation of surface pressure coefficient on NACA 4412 baseline.

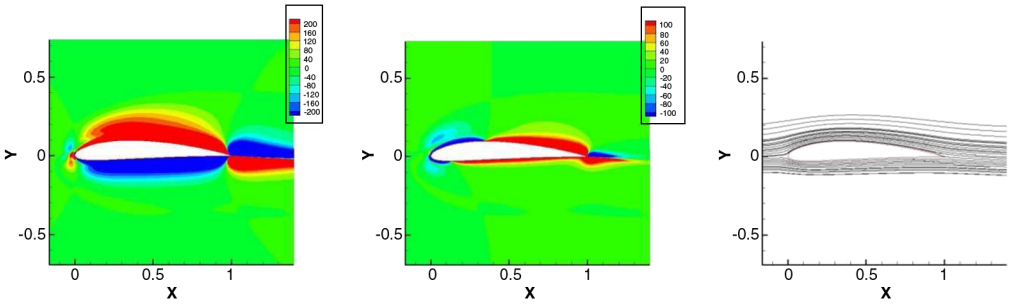

a) NACA4412 baseline

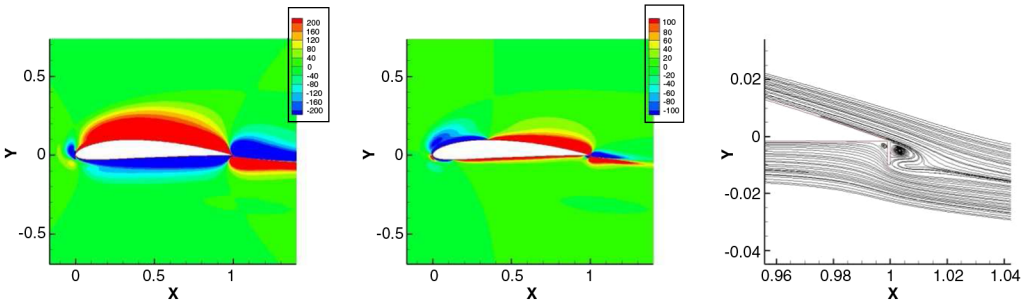

b) NACA4412+ a gurney flap (1% chord length)

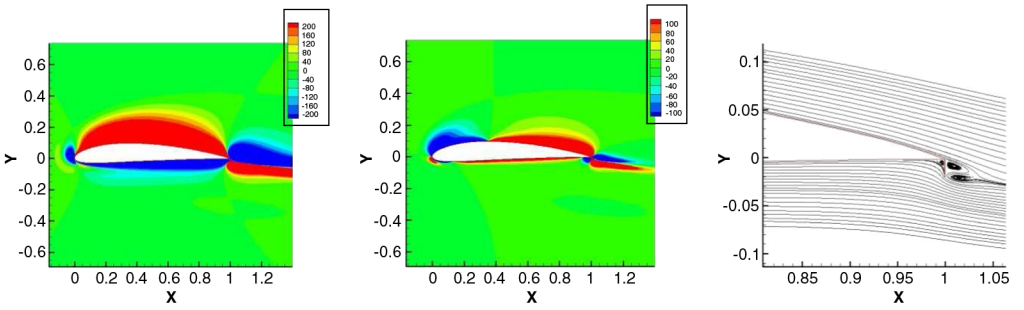

c) NACA4412+ a gurney flap (2% chord length)

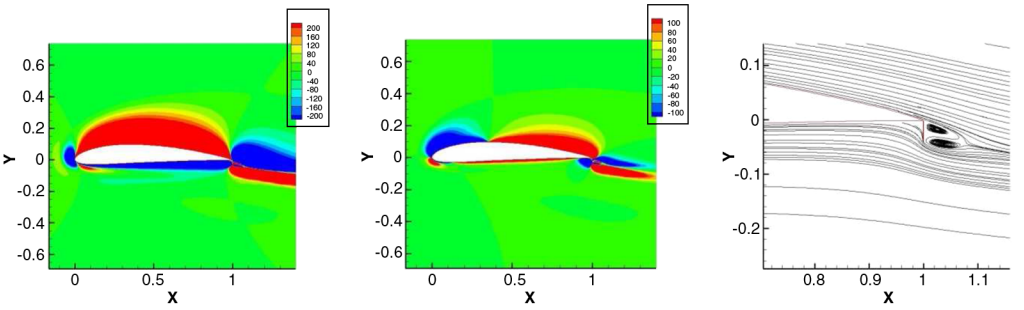

d) NACA4412+ a gurney flap (4% chord length)

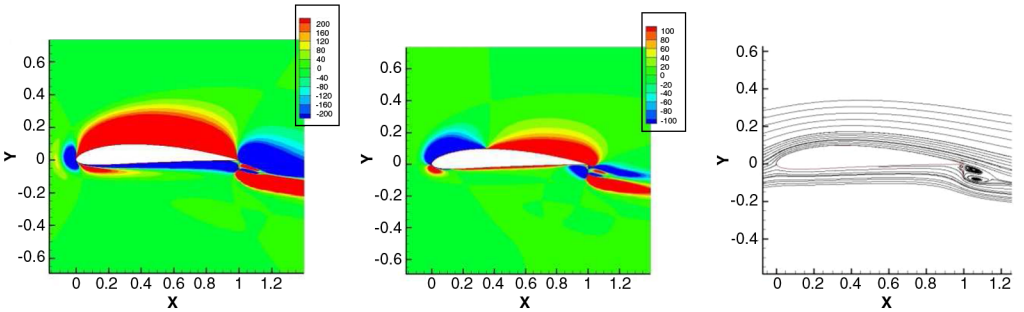

e) NACA4412+ a gurney flap (7% chord length)

Fig. 2 Contour plots of lift force (left), drag force (middle), and streamline (right).

well known, the presence of the Gurney flap increases the upper surface suction and the lower surface pressure, causing increment loading along the entire length of airfoil, noticeably near the trailing edge. The addition of Gurney flap causes downward turning of the flow behind the Gurney flap. Figure 2 shows the evolution of positive parts and negative parts of the lift and drag elements' density contours for different flap sizes. The addition of a Gurney flap is shown to enhance lift, due to the increase of the positive lift-element distribution on the suction side of the airfoil and inside the flowfield behind the flap and due to the negative lift-element distribution on the lower surface of the airfoil and the flap for the test cases. Note that the amount of positive lift elements in the flowfield is gradually increasing and the amount of negative lift element becomes less as the flap size becomes larger. On the other hand, from the drag elements' contour plots, the Gurney flap enhances the negative contributions to the drag force on the suction surface near the leading edge of the main airfoil and the lower surface of the trailing edge near the corner. However, the Gurney flap increases the positive contributions of the drag inside two counter-rotating vortices downstream of the flap. It is interesting to observe that negative drag elements emerge from a region extending a short distance downstream of the leading edge of the airfoil. A growing wake appearing in the flow regime behind the Gurney flap and the zone of recirculation also provides negative drag elements downstream of the main airfoil, but contributes positive drag elements in flowfields just behind the flap.

To get further understanding of the mechanism of the Gurney flap, we can analyze the decomposition of lift and drag into contributions of the volume and surface force elements, as given in Tables 1 and 2. Table 1 shows that increasing Gurney flap size enhances the lift over the entire computed range. It is also shown that the increased lift largely results from effect of the vorticity within the flow volume (C_{Lv}), including the flow separation behind the flap or far away from the airfoil. Meanwhile, the surface vorticity contribution C_{Ls} also increases significantly, though it contributes a smaller part of the lift. From Table 2, it is very interesting to see that the volume vorticity still plays a major role in the increase of drag force no matter how large the flap size is, yet the surface vorticity contributes a negative source of drag force at the cases of flap sizes from 1 to 4%, reducing the total drag force below the clean-airfoil value when the flap size is 1 and 2%. There is no significant increase in the total drag force if the Gurney flap height is kept less than 2% chord. When the flap size is near or larger than 4% chord length, contribution of negative drag elements by the surface vorticity disappears. Note that positive drag is net-produced on the airfoil when the Gurney flap size is larger than 4% of the chord length.

Table 1 Contributions to the lift coefficient by the lift elements at different flap sizes

Gurney flap size	C_L	C_{Ls}	C_{Lv}
Clean	0.270607074	0.050826037	0.219781037
1%	0.68236871	0.165385491	0.516983219
2%	0.84558283	0.222246815	0.623336015
4%	1.0108742	0.269628958	0.741245242
7%	1.1279781	0.28597005	0.84200805

Table 2 Contributions to the drag coefficient by the drag elements at different flap sizes

Gurney flap size	C_D	C_{Ds}	C_{Dv}
Clean	0.065288564	0.021775429	0.04351314
1%	0.039091713	−0.010941536	0.050033239
2%	0.045996289	−0.011701722	0.057698011
4%	0.076345883	−0.005856243	0.082202126
7%	0.10685768	0.02470202	0.082155661

Table 3 Predicted lift-to-drag ratio at different flap sizes

Gurney flap size	Lift-to-drag ratio
Clean	4.145
1%	17.456
2%	18.384
4%	13.241
7%	10.556

Conclusions

Here, the force-element method gives us a better understanding of why the highest lift-to-drag ratio occurs at the flap size of around 2% of chord, as shown in Table 3. The main reasons are found as follows:

1) The Gurney flap of 2 % chord increases drastically the lift, due to the volume as well as surface vorticity, compared to the clear airfoil.

2) The flap produces a negative drag source from surface vorticity to substantially cancel out the drag coming from the volume vorticity.

Regarding the lift-to-drag ratio, these effects are also observed for the cases of 1 and 4% flaps, but intensified when the flap chord is at 2%. In other words, for either drag or lift, the volume vorticity contributes much more than the surface vorticity, but it is the latter that plays a key role in optimizing the lift-to-drag ratio by contributing oppositely to the lift and drag. The presented force-element distributions show that the addition of the Gurney flap produces a significant positive source of lift over the suction side of the airfoil, due to both surface and volume vorticity effects. The positive contributions to lift and the negative contributions to drag produced by the Gurney flap are clearly shown in the analysis of surface and volume vorticity effects.

Acknowledgments

We acknowledge financial support from the National Science Council under the project NSC 97-2221-E-216-009-MY2 and the computer facility supported by the National Center for High-Performance Computing, Hsin-Chu, Taiwan, Republic of China.

References

[1] Niu, Y. Y., "MUSCL Type Limiters for Flux Splitting Methods and Applications," Ph.D. Dissertation, Ohio State Univ., Columbus, OH, Aug. 1995.

[2] Stratford, B. S., "The Prediction of Separation of the Turbulent Boundary Layer," *Journal of Fluid Mechanics*, Vol. 5, No. 1, Jan. 1959, pp. 1–16. doi:10.1017/S0022112059000015

[3] Smith, A. M. O., "High-Lift Aerodynamics," *Journal of Aircraft*, Vol. 12, No. 6, June 1975, pp. 501–530. doi:10.2514/3.59830

[4] Leibeck, R. H., "Design of Subsonic Airfoils for High Lift," *Journal of Aircraft*, Vol. 15, No. 9, Sept. 1978, pp. 547–561. doi:10.2514/3.58406

[5] Wadcock, A., "Investigations of Low-Speed Turbulent Separated Flow Around Airfoils," NASA CR 177450, Aug. 1987.

[6] Storms, B. L., and Jang, C. S., "Lift Enhancement of an Airfoil Using a Gurney Flap and Vortex Generators," AIAA Paper 93-0647, Jan. 1993.

[7] Jang, C. S., Ross, J. R., and Cummings, R. M., "Numerical Investigation of an Airfoil with a Gurney Flap," *Aircraft Design*, Vol. 1, No. 2, June 1998, pp. 75–88. doi:10.1016/S1369-8869(98)00010-X

[8] Jeffrey, D., Zhang, X., and Hang, D. W., "Aerodynamics of Gurney Flaps on a Single-Element High-Lift Wing," *Journal of Aircraft*, Vol. 37, No. 2, 2000, pp. 295–301. doi:10.2514/2.2593

[9] Solovitz, S., and Eaton, J., "Spanwise Response Variation for Partial-Span Gurney-Type Flaps," *AIAA Journal*, Vol. 42, No. 8, 2004, pp. 1640–1643. doi:10.2514/1.770

[10] Solovitz, S., and Eaton, J., "Dynamic Flow Response Due to Motion of Partial-Span Gurney-Type Flaps," *AIAA Journal*, Vol. 42, No. 9, 2004, pp. 1729–1736. doi:10.2514/1.1200

[11] Niu, Y. Y., and Liou, M. S., "Numerical Simulation of Dynamic Stall

Using an Improved Advection Upwind Splitting Method," *AIAA Journal*, Vol. 37, No. 11, 1999, pp. 1368–1392.

[12] Niu, Y. Y., and Tsai, W. F., "Aerodynamic Analysis of High-Lift Airfoils by a Dual Time Integration Method with Upwind Splitting," *High Performance Computing on the Information Superhighway*, IEEE Computer Society, Washington, D.C., April 1997, pp. 266–270. doi:10.1109/HPC.1997.592158

[13] Chang, C. C., "Potential Flow and Forces for Incompressible Viscous Flow," *Proceedings of the Royal Society of London A*, Vol. 437, 1992, pp. 517–525. doi:10.1098/rspa.1992.0077

[14] Chang, C. C., Yang, S. H., and Chu, C. C., "A Many-Body Force Decomposition with Applications to Flow About Bluff Bodies," *Journal of Fluid Mechanics*, Vol. 600, 2008, pp. 95–104.

[15] Landau, L. D., and Lifshitz, E. M., *Fluid Mechanics*, 2nd ed., Butterworth-Heinemann, Oxford, Jan. 1987.

A. Tumin
Associate Editor